An implementation method based on ERS imaging mode for sun sensor with 1 kHz update rate and 1″ precision level

Minsong Wei,[1,2,3] Fei Xing,[1,2,3,*] and Zheng You[1,2,3]

[1]*Department of Precision Instrument, Tsinghua University, Beijing 100084, China*
[2]*State Key Laboratory of Precision Measurement Technology and Instruments, China*
[3]*Collaborative Innovation Center for Micro/Nano Fabrication, Device and System, China*
[*]*xingfei@mail.tsinghua.edu.cn*

Abstract: Stringent attitude determination accuracy through a high bandwidth is required for the development of the advanced space technologies, such as earth observation and laser communication. In this work, we presented a novel proposal for a digital sun sensor with high accuracy, large Field of View (FOV) and ultra-high data update rate. The Electronic Rolling Shutter (ERS) imaging mode of an APS CMOS detector was employed and an "amplifier factor" was introduced to improve the data update rate significantly. Based on the idea of the multiplexing detector, a novel mask integrated with two kinds of aperture patterns was also introduced to implement its distinctive performance of high precision and large FOV. Test results show that the ERS based sun sensor is capable of achieving the data update rate of 1 kHz and precision of 1.1″ (1σ) within a 105° × 105° FOV. The digital sun sensor can play an important role in precise attitude determination and provide a broader application for high accuracy satellites.

OCIS codes: (120.6085) Space instrumentation; (120.4640) Optical instruments; (040.1880) Detection.

References and links

1. E. H. Anderson, J. P. Fumo, and R. S. Erwin, "Satellite ultraquiet isolation technology experiment (SUITE)," in *Proceedings of IEEE Conference on Aerospace* (Institute of Electrical and Electronics Engineers, Big Sky, MT, 2000), pp. 299–313.
2. F. H. Bauer and W. Dellinger, "Gyroless fine pointing on small explorer spacecraft," in *Proceedings of the AIAA Guidance, Navigation and Control Conference*, (American Institute of Aeronautics and Astronautics, Monterey, CA, 1993), pp. 492–506.
3. C. W. Hindman, S. L. Lacy, and N. Hatten, "Image Based Acquisition and Tracking for Multi-Access Laser Communications," in *Proceedings of IEEE Conference on Aerospace* (Institute of Electrical and Electronics Engineers, Big Sky, MT, 2006), pp. 1–10.
4. T. Iwata, "Precision attitude and position determination for the Advanced Land Observing Satellite (ALOS)," Proc. SPIE **5659**, 34–50 (2005).
5. H. Huo, M. Ma, Y. Li, and J. Qiu, "The application of MHD angular rate sensor in aerospace," Vac. Cryogenics **17**(2), 114–120 (2011).
6. G. D. Rogers, M. R. Schwinger, J. T. Kaidy, T. E. Strikwerda, R. Casini, A. Landi, R. Bettarini, and S. Lorenzini, "Autonomous star tracker performance," Acta Astronaut. **65**(1–2), 61–74 (2009).
7. W. Zhang, W. Quan, and L. Guo, "Blurred Star Image Processing for Star Sensors under Dynamic Conditions," Sensors (Basel) **12**(12), 6712–6726 (2012).
8. T. Sun, F. Xing, Z. You, and M. Wei, "Motion-blurred star acquisition method of the star tracker under high dynamic conditions," Opt. Express **21**(17), 20096–20110 (2013).
9. S. Mobasser and C. C. Liebe, "MEMS based sun sensor on a chip," in *Proceedings of IEEE Conference on Control Applications* (Institute of Electrical and Electronics Engineers, Istanbul, 2003), pp. 1483–1487.
10. C. Zhang, P. Cui, and Z. Yang, "A design method of the sun snesor used on the miniature spinning satellite," Deep Space Explor. **1**, 34–37 (2008).
11. C. W. de Boom, J. A. P. Leijtens, L. M. H. v.Duivenbode, and N. van der Heiden, "Micro digital sun sensor: System in a package," in *Proceedings of IEEE Conference on MEMS, NANO and Smart Systems* (Institute of Electrical and Electronics Engineers, Banff, Alberta, 2004), pp. 322–328.

#197267 - $15.00 USD Received 16 Sep 2013; revised 16 Dec 2013; accepted 17 Dec 2013; published 23 Dec 2013

12. J. Enright, D. Sinclair, and C. Li, "Embedded algorithms for the SS-411 digital sun sensor," Acta Astronaut. **64**(9-10), 906–924 (2009).
13. P. Ortega, G. López-Rodríguez, J. Ricart, M. Domínguez, L. M. Castañer, J. M. Quero, C. L. Tarrida, J. Garcia, M. Reina, A. Gras, and M. Angulo, "A miniaturized two axis sun sensor for attitude control of nano-satellites," IEEE Sens. J. **10**(10), 1623–1632 (2010).
14. M. S. Wei, F. Xing, B. Li, and Z. You, "Investigation of Digital Sun Sensor Technology with an *N*-Shaped Slit Mask," Sensors (Basel) **11**(12), 9764–9777 (2011).
15. N. Xie, A. J. Theuwissen, B. Büttgen, H. Hakkesteegt, H. Jasen, and J. Leijtens, "Micro-digital sun sensor: An imaging sensor for space applications," in *Proceedings of IEEE Conference on Industrial Electronics* (Institute of Electrical and Electronics Engineers, Bari, 2010), pp. 3362–3365.
16. C. De Boom and N. Van Der Heiden, "A novel digital sun sensor: Development and qualification for flight," in *Proceedings of 54th International Astronautical Congress*, (International Astronautical Federation, Bermen, 2003), pp. 708–715.
17. F. Xing, Z. You, G. Zhang, and J. Sun, "A novel active pixels sensor (APS) based sun sensor based on a feature extraction and image correlation (FEIC) technique," Meas. Sci. Technol. **19**(12), 125203 (2008).
18. J. Gu, Y. Hitomi, T. Mitsunaga, and S. Nayar, "Coded rolling shutter photography: Flexible space-time sampling," in *Proceedings of IEEE Conference on Computational Photography* (Institute of Electrical and Electronics Engineers, Bari, 2010), pp. 1–8.
19. M. Meingast, C. Geyer, and S. Sastry, "Geometric models of rolling-shutter cameras," in *Proceedings of Omnidirectional Vision, Camera Networks and Non-classical Cameras*, (Beijing, 2005), pp. 12 –19.
20. M. Wany and G. P. Israel, "CMOS image sensor with NMOS-only global shutter and enhanced responsivity," IEEE Trans. Electron. Dev. **50**(1), 57–62 (2003).
21. F. J. Delgado, J. M. Quero, J. Garcia, C. L. Tarrida, P. R. Ortega, and S. Bermejo, "Accurate and Wide-Field-of-View MEMS-Based Sun Sensor for Industrial Applications," IEEE. Trans. Ind. Electron. **59**(12), 4871–4880 (2012).
22. C. Hersom, R. Berman, J. Shah, and R. Hornsey, "Digital sun sensor using multiple pinholes," in *Proceedings of CASI Conference on Astronautics*, (Canadian Aeronautics and Space Institute, Ottawa, 2002), pp. 12–14.
23. R. Strietzel, "Two-dimensional calibration of a sun attitude sensor," in *Proceedings of 15th International Federation of Automatic Control Triennial World Congress on Automatic Control*, (IFAC, Barcelona, 2002), pp. 259–264.

1. Introduction

The requirements for attitude determination systems are becoming more and more stringent as the advanced earth observation satellites and long-range laser links for satellite communications are currently under rapid development [1–4]. For instance, in order to obtain high-resolution earth observation images with precise geometric accuracy, fine pointing, attitude and position determination for earth observation satellites is essential. In addition, due to the difficulty of establishment of laser communication link, it is also important to achieve the satellite stability with extremely high requirements, which is also based on a precise attitude measurement and determination. Therefore, arc-second class attitude measurement accuracy and extended attitude determination bandwidth from less than 1Hz up to 500 Hz are required for the sensors in the attitude determination system [5].

Currently, the high attitude measurement accuracy is primarily accomplished by the star tracker [1]. However, the star tracker will malfunction when it is under dynamic conditions and it has a low update rate of several Hertz, resulting from its long exposure time [6–8]. Compared to the star tracker, the sun sensor, another essential component of satellites, has many advantages such as low power consumption, small size and weight [9]. Furthermore, due to the brightness of the sun, the exposure time of the sun sensor could be extremely short and hence it will function well under dynamic conditions [10]. Moreover, the short exposure time makes the high update rate of up to several kilo-Hertz possible for the sun sensor, while such a high update rate is impossible for the star tracker. Thus, the sun sensor has more development potentials and research on digital sun sensors as well as related products has substantially grown in recent years [11–17]. Nevertheless, the accuracy of those sun sensors is maximum 0.02° and the average data update rate is only dozens of Hertz, neither of which satisfies the requirements discussed above.

Improving the performance of the sun sensor to make it qualified for the stringent attitude measurement accuracy with high update rate is of great interest in this research. We present a novel digital sun sensor with 1 kHz update rate as well as high precision. This sun sensor is composed of a dedicated mask with two kinds of apertures on it and a planar CMOS image

#197267 - $15.00 USD Received 16 Sep 2013; revised 16 Dec 2013; accepted 17 Dec 2013; published 23 Dec 2013

sensor, which works in the ERS mode to achieve the update rate of 1 kHz. The precision is 1.1 arc-second (1σ) and its FOV is 105° × 105°.

2. Approach for update rate improvement based on ERS

2.1 Operation principle of ERS

Electronic Rolling Shutter (ERS) is regularly applied by CMOS image sensors as a method of image acquisition, in which the exposure of an image area is conducted line by line [18–20]. Due to the line-by-line exposure pattern, noticeable image distortion will appear. However, compared with the Global Shutter (GS) in which the whole image is exposed simultaneously, ERS provides an outstanding performance in terms of SNR and better sensitivity. In addition, it is possible to achieve the goal of ultra-high update rate based on ERS.

Figure 1 shows the operating mode of ERS and GS. In GS mode, every line in the whole image frame is exposed simultaneously from $t = 0$ and then the image is read out line by line. The next frame will be exposed after the data readout of the last line is finished. Thus, considering a CMOS sensor with n lines, its frame period $t_{F\text{-}GS}$ is determined by Eq. (1):

$$t_{F-GS} = t_{INT} + n \times t_{RD} + t_{WT}, \tag{1}$$

Where, t_{INT} is the exposure time or the integration time; t_{RD} is the data readout time of each line and t_{WT} is the wait time between two frames.

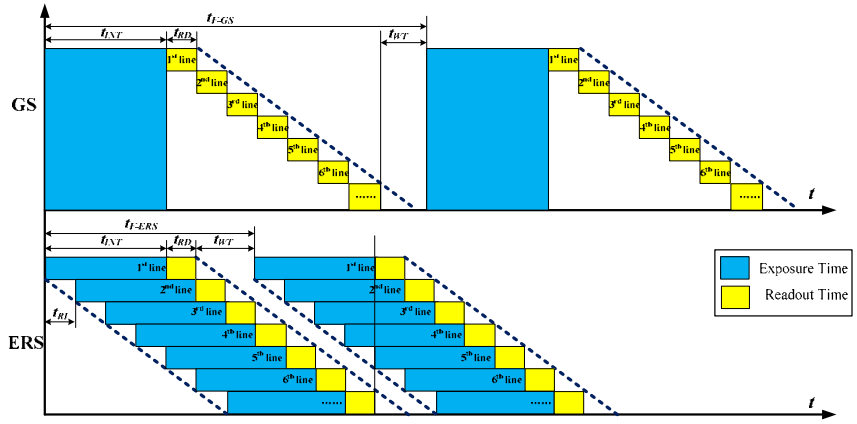

Fig. 1. Operation mode of GS and ERS.

The exposure mode in ERS is completely different with that in GS. Each line of the image area is exposed successively from top to bottom in ERS mode. That is, at the moment $t = 0$, only the pixels of the first line begin exposing, and then after a given interval t_{RI}, the following line will begin exposing, so on and so forth. So $t_{F\text{-}ERS}$, the frame period in ERS mode is determined by Eq. (2):

$$t_{ERS} = t_{INT} + t_{RD} + t_{WT}. \tag{2}$$

In ERS mode, although each line has the same and configurable exposure time t_{INT}, the initial exposure moment of every line t_{ST} is asynchronous. Consequently, the instantaneous information contained in every line is different. Using ERS, the data output of the digital sun sensor will update every time the data of a line is readout. In addition, the interval between the initial moments of two adjacent lines is identical and tunable. Therefore, we have Eq. (3)-(5) as the foundations of our approach for our novel digital sun sensor with 1 kHz update rate:

$$t_{INT1} = t_{INT2} = \cdots = t_{INTi} = \cdots = t_{INTn}, \tag{3}$$

$$t_{RI1} = t_{RI2} = \cdots = t_{RIi} = \cdots = t_{RI(n-1)}, \tag{4}$$

#197267 - $15.00 USD Received 16 Sep 2013; revised 16 Dec 2013; accepted 17 Dec 2013; published 23 Dec 2013

$$t_{RI} = t_{RD}, \tag{5}$$

Where t_{INTi} is the exposure time of line i and t_{RTi} is the interval between the initial moments of line i and line $i + 1$.

2.2 Approach for kHz class update rate achievement

Conventionally, data output of a digital sun sensor updates after the acquisition of a full frame when the image sensor is working in GS mode. This is because the whole image frame is exposed simultaneously and thus each sun spot that is used to calculate and determine the attitude has the same instantaneous attitude information. So the data update rate of a digital sun sensor utilizing GS would be limited by $t_{F\text{-}GS}$.

Considering a frame of image taken in ERS mode, every line of the image has a different initial moment, which means that the exposure of different lines begins at a disparate time. If there are distinguished sun spots scattering in different lines, each sun spot could be used for a certain instantaneous attitude determination. Specifically, if there are (k-j + 1) sun spots located in different lines during the period from $t = t_j$ to $t = t_k$, there will be m sun spots in the whole image frame, as shown in Fig. 2. As the attitude information varies from line to line, the output of the digital sun sensor will be updated m times during one frame period and hence the data update rate f_{ERS} can be expressed by Eq. (6).

$$f_{ERS} = \frac{m}{t_{F-ERS}} = m \cdot f_{F-ERS}, \tag{6}$$

Where $f_{F\text{-}ERS}$ is the frame update frequency in ERS mode, and m can be referred to as the "amplifier factor" since the data update rate in ERS mode could be amplified by m times.

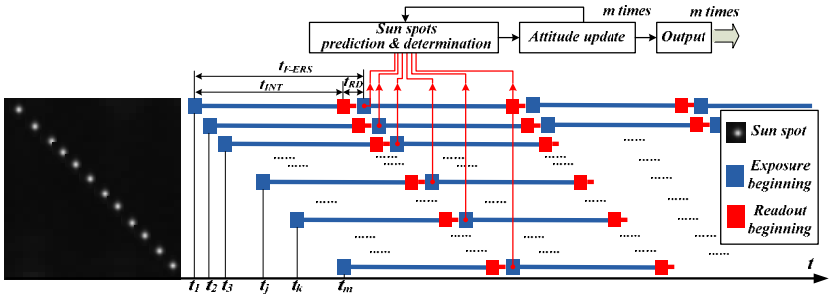

Fig. 2. Timing and operation flow of the ERS based digital sun sensor.

The timing optimization is carried out to minimize the frame period and thus to achieve the maximum f_{ERS}. To accomplish this goal, t_{WT} is set to zero and the exposure time is set through Eq. (7):

$$t_{INT} = (n-1)t_{RD}. \tag{7}$$

The readout of the next line starts immediately when the readout of the current line is completed. In this case, every line has the same exposure time while the initial moment is delayed successively with a fixed interval and the assembly-lined readout of the image frame is achieved.

Generally, there are approximately 1000 lines in a CMOS sensor, so the basic optimized data update rate of the novel digital sun sensor can be calculated by Eq. (8):

$$f_{ERS} = \frac{m(n-1)}{n} \cdot \frac{1}{t_{INT}} \approx \frac{m}{t_{INT}}. \tag{8}$$

Based on Eq. (8), an ERS based digital sun sensor has the distinctive capability of kHz class update rate resulting from the short exposure time (t_{INT} is approximately several dozens of milliseconds) and the large amount of the sun spots scattering in different lines (m could be

#197267 - $15.00 USD Received 16 Sep 2013; revised 16 Dec 2013; accepted 17 Dec 2013; published 23 Dec 2013

several dozens). Due to the ERS mode, the "amplifier factor" m is introduced to increase the update rate of the digital sun sensors by one or two orders of magnitude.

The operation flow of the digital sun sensor based on ERS is also briefly demonstrated in Fig. 2. Each determined sun spot is used to calculate the incident angles of the sun light and predict the next sun spot. The operation procedure based on ERS mode starts when the first sun spot is located. Thereafter the output data containing attitude information will update every time a new sun spot is determined. During a frame period, the data will update m times when there are m sun spots in one image frame.

3. High resolution and large FOV based on multiplexing detector

Based on the principle of the digital sun sensor, as shown in Fig. 3(a), the trade-off between large FOV and high resolution has always hindered the improvement of the resolution of the digital sun sensor with a large FOV [21]. In general, the FOV and resolution d_α can be calculated by Eq. (9) and (10).

$$d_\alpha = \cos^2\alpha \cdot \frac{d_{\Delta l}}{h}, \tag{9}$$

$$FOV = 2\arctan\left(\frac{l_{sensor}}{2h}\right), \tag{10}$$

where α denotes the incident angle; h denotes the distance between the mask plane and the focal plane; l_{sensor} denotes the size of the image sensor and $d_{\Delta l}$ denotes the distance resolution of the image sensor.

Apparently, the resolution is proportional to h while FOV is inversely proportional to h. In this case, if a higher resolution could be achieved with a larger h in Eq. (9), the FOV would become smaller based on Eq. (10) and vice versa.

Thus, utilization of the fish-eye lens or multiple pinholes in a dome has been proposed to get a larger FOV [16, 22]. However, there are still significant drawbacks such as increment of system complexity or increment of difficulty of manufacture and assemble. What is more, neither of the above proposals could be used for the goal of ultra-high date update rate. Therefore, we propose an innovative mechanism based on a multiplexing detector and a mask with two kinds of aperture patterns. As shown in Fig. 3(b), only one multiplexing detector and one mask will be used in our design. The whole FOV is composed of several overlaid sub-FOVs and each sub-FOV can be indicated by distinguished mark patterns on the mask. Figure 3 shows that using a multiplexing detector, h could be enlarged without decreasing the FOV, and thus it results in a higher resolution.

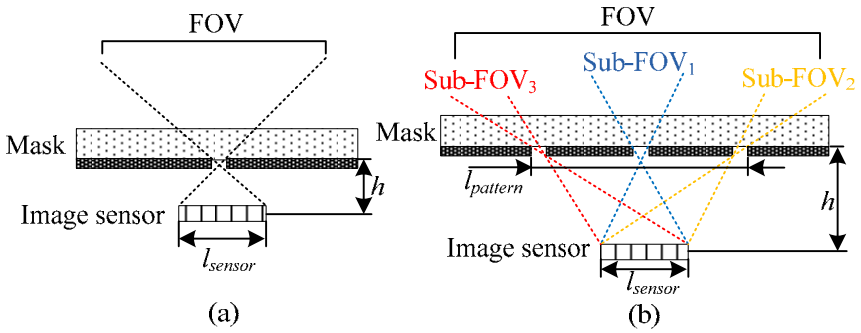

Fig. 3. Schematic of FOV of the digital sun sensor without multiplexing detector (a) and with multiplexing detector (b).

FOV of the sun sensor with the novel mask and multiplexing detector can be calculated by Eq. (11) which is derived from Eq. (10):

#197267 - $15.00 USD Received 16 Sep 2013; revised 16 Dec 2013; accepted 17 Dec 2013; published 23 Dec 2013

$$FOV = 2\arctan\left(\frac{l_{pattern} + l_{sensor}}{2h}\right), \tag{11}$$

where $l_{pattern}$ and l_{sensor} denote the size of the image sensor and the pattern on the mask, respectively.

Compared to Eq. (10), since $l_{pattern}$ can be great larger than l_{sensor}, it is obvious that FOV would be broaden significantly with a determined h. Therefore, the innovative design will dramatically improve the resolution of the sun sensors without sacrificing the FOV and there are no additional optical lenses or other structures needed.

4. Implementation of the novel sun sensor

To achieve the goal of arc-sec class resolution, h = 17.2 mm has been calculated based on Eq. (9). And a 47.5 mm × 48.8 mm pattern area is required to realize a 105° × 105° FOV based on Eq. (10), given the active area of the image sensor is 6.78 mm × 5.43 mm. The crucial component of the sun sensor is the mask which comprises two different patterns of apertures, as shown in Fig. 4(a). Essentially, the shape of these two kinds of apertures is square, and the only difference is the way they are arranged. Due to the large distance between the mask plane and the focal plane, diffraction is no longer negligible and has to be analyzed. We have conducted numerical simulations to optimize the aperture size and the clearence between the image spots of adjacent apertures. The simulation results suggest that the size of diffraction spot approaches its minimum when the aperture is 116.6um × 116.6um and the clearence is 424um.

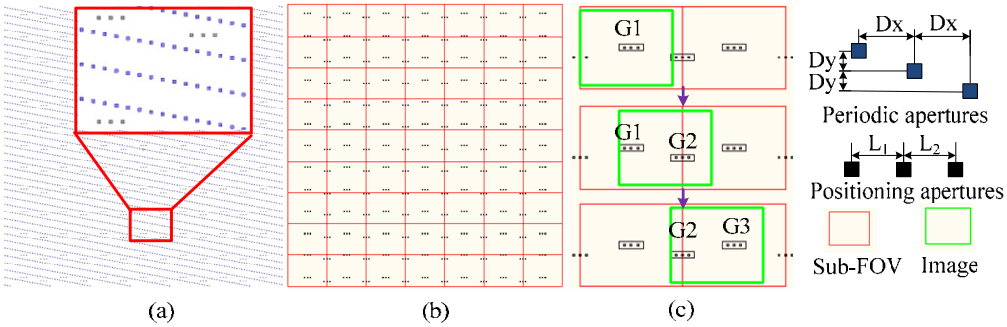

Fig. 4. The schematic of the mask design with detail view (a), the division of sub-FOVs (b) and sub-FOV discrimination (c).

The apertures in black function as “positioning apertures” which are used to determine the sub-FOVs. Every group of positioning apertures is composed of three apertures with distance information. Here, we assume that L_1 is the distance between the left and middle apertures and L_2 is the distance between the right and middle apertures; they are both in the unit of pixel length. Thus, every group will be distinguished from each other as every set of (L_1, L_2) is coded uniquely, such as (80, 80) for the central group of positioning apertures, (80, 81) for the group to the left of the central group and (81, 80) for the group just above the central group. The area of a sub-FOV is equal to the sensor area, thus, the 47.5 mm × 48.8 mm pattern area is divided into 7 × 9 sub-FOVs, as shown in Fig. 4(b). Furthermore, the positioning apertures are mapped elaborately to ensure that there will be at least one group of positioning apertures in every sub-FOV. It is illustrated in Fig. 4(c). At the beginning, a certain sub-FOV is determined by a group of positioning apertures, G1; and then, with the incident sun angles moving toward to the next sub-FOV range, the previous sub-FOV which is determined by G1will be determined by next group G2 or G3. In such case, there is no gap between sub-FOVs and all incident sun angles within the whole FOV will be determined successfully.

The other kind of apertures in blue are referred to as “periodic apertures” because they appear periodically and every aperture of this kind is used to calculate the instantaneous

#197267 - $15.00 USD Received 16 Sep 2013; revised 16 Dec 2013; accepted 17 Dec 2013; published 23 Dec 2013

incident sun angles after a sub-FOV is successfully determined. In this case, the "amplifier factor" m is essentially determined by these two parameters, Dx and Dy. Based on the current design, there are at least 64 determined periodic sun spots in one frame, so m is equal to 64. In the ERS mode, with $f_{F\text{-}ERS}$ = 16 Hz, the 1.0 kHz data update rate is achieved based on Eq. (6).

The sun sensor is mainly composed of the mask which is fabricated by MEMS procedures, the housing as well as the electrical system. The mask is constrained and aligned to the image sensor between the housing body and a cover and the assembly of the digital sun sensor is shown in Fig. 5.

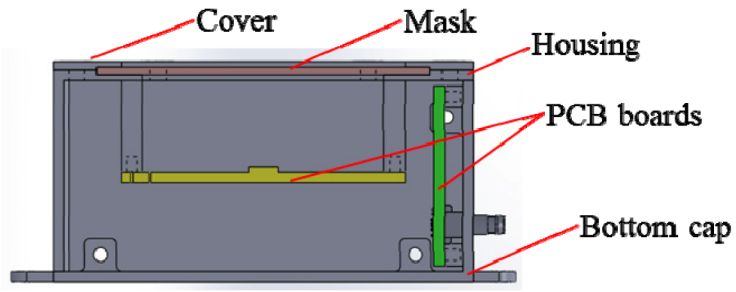

Fig. 5. Cross sectional view of the sun sensor

5. Experiments and results

Experiments have been carried out to test the performance of the prototype digital sun sensor which is shown in Fig. 6. The test system includes a sun simulator and a three-axis gimbals rotary table with the position accuracy of 0.0001°, as shown in Fig. 7. The sun simulator can provide the collimated light with the brightness of 1/10 sun constant. The sun sensor prototype was fixed on the rotary table and arbitrary sun incident angles can be established with the rotation of the three-axis gimbals rotary table.

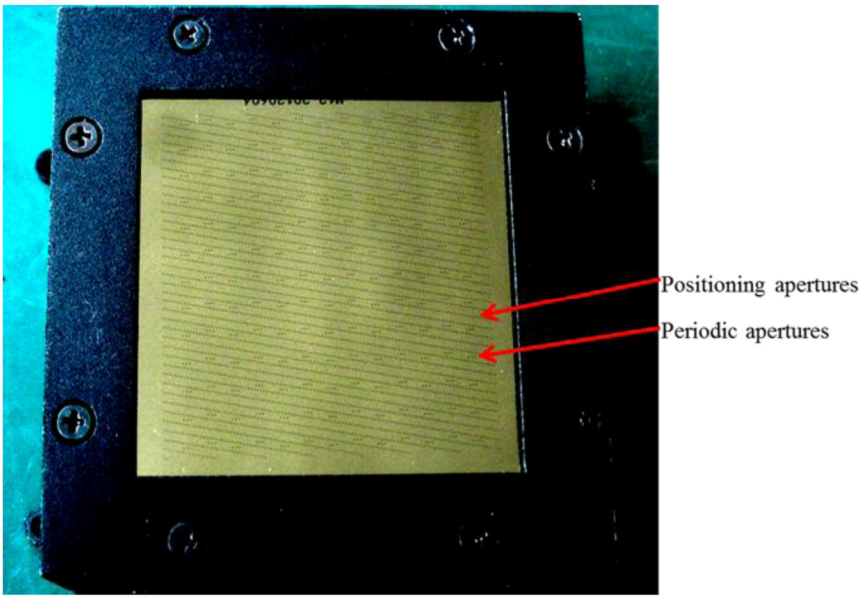

Fig. 6. Prototype of the sun sensor.

#197267 - $15.00 USD Received 16 Sep 2013; revised 16 Dec 2013; accepted 17 Dec 2013; published 23 Dec 2013

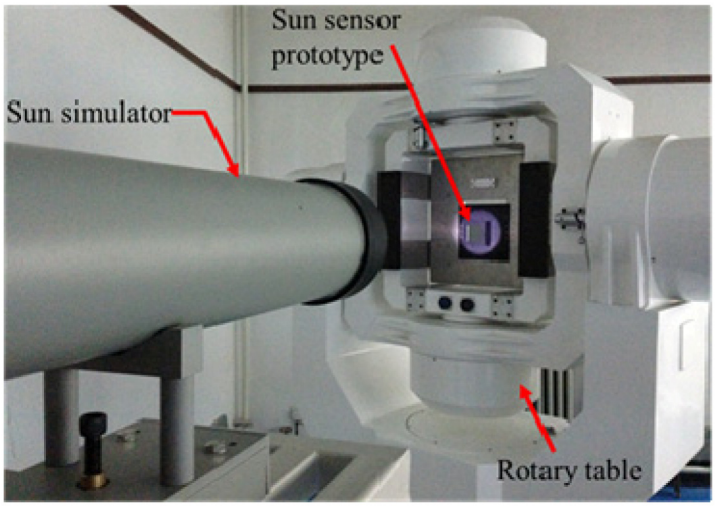

Fig. 7. Test system for the sun sensor prototype.

5.1 ERS imaging effect under dynamic conditions

Two image frames of sun spots taken by the image detector are shown in Fig. 8 to demonstrate the principle of ERS. Figure 8(a) is the image taken at static state while Fig. 8(b) is the image taken at dynamic state. These two states are depicted in the right part of Fig. 8. At static state, the incident sun light goes through the mask at a certain angle and thus every sun spot in the image we taken is arranged as the apertures designed. Under the dynamic condition, the incident sun light goes through the mask with an increasing incident angle. It is equivalent to the situation that the incident angle of the sun light and the image sensor is fixed with the mask moving above the image sensor.

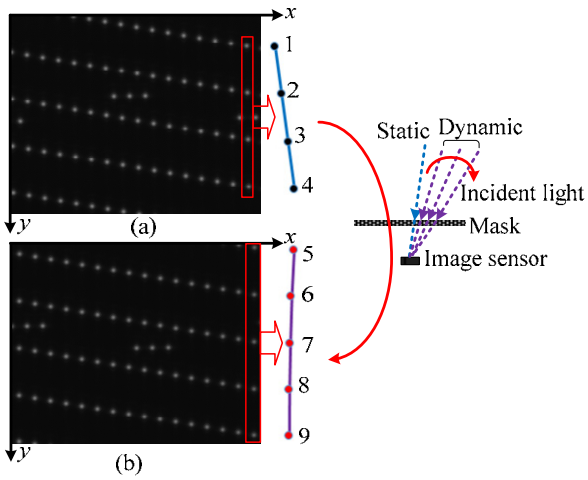

Fig. 8. The sun spots image taken by CMOS detector at static state (a) and at dynamic state (b).

The last columns of the sun spots in both images have been extracted and numbered from 1 to 9, as shown in Fig. 8. The center coordinates of these sun spots have been calculated and Table 1 is the location information of the extracted sun spots. At static state, the sun spots in the same column lean downwards to the right according to the calculated location information of sun spots 1 ~4 and this is revealed schematically by the blue line shown in Fig. 8(a). On the contract, according to the location information of the sun spots 5 ~9, the sun spots in the same

#197267 - $15.00 USD Received 16 Sep 2013; revised 16 Dec 2013; accepted 17 Dec 2013; published 23 Dec 2013

column lean downwards to the left at dynamic state, shown as the purple line in Fig. 8(b). This is because the initial exposure moment of upper sun spot is earlier than that of lower sun spot in ERS mode. Therefore, under dynamic conditions, compared with the upper sun spots, the lower sun spots will move a certain distance along the moving direction until they start exposing. Given the equivalent moving direction is inverse to the positive direction of *x*-axis in this test, the change in slope from static state to dynamic state coincides exactly with the analyzed moving direction, and every sun spot can be used to calculate the instantaneous incident sun angle. Thus, our test results demonstrate that the principle of ERS can be successfully employed to achieve the kHz class update rate and the novel sun sensor is capable of functioning under dynamic conditions.

Table 1. Location information of sun spots abstracted in ERS principle test

Index	Cs[a]	Lr[b]
1	(1204.03, 161.66)	75.97
2	(1207.66, 401.62)	72.34
3	(1211.30, 641.55)	68.70
4	(1214.95, 881.67)	65.05
5	(1243.44, 17.29)	36.56
6	(1242.16, 257.23)	37.84
7	(1241.37, 497.27)	38.63
8	(1240.89, 737.20)	39.11
9	(1240.76, 977.15)	39.24

[a]The center coordinates of the sun spot.
[b]The distance between the sun spot and the right edge of the image.

5.2 Performance experiments

To demonstrate the performance of the prototype of the digital sun sensor, one quadrant of the whole FOV was measured and the centroiding algorithm was utilized to extract the sun spots. The sun sensor prototype was fixed onto the rotary table and then was adjusted to be collinear with the sun simulator. Then, the rotary table was rotated through one quadrant of the 105° × 105° FOV with the step of 0.5°along two axes and the step of 5°otherwise. The measured values corresponding to the theoretical incident angles were employed to analyze the system error and calibrate the system [23].

The performance experiment indicates that the digital sun sensor operates well in accordance with the design proposal and the precision is 1.1″ (1σ), as shown in Fig. 9. Further tests demonstrate that the data update rate reached 1 kHz at the frame frequency of 16 fps. It can be greatly improved by increasing the frame frequency of the CMOS image detector.

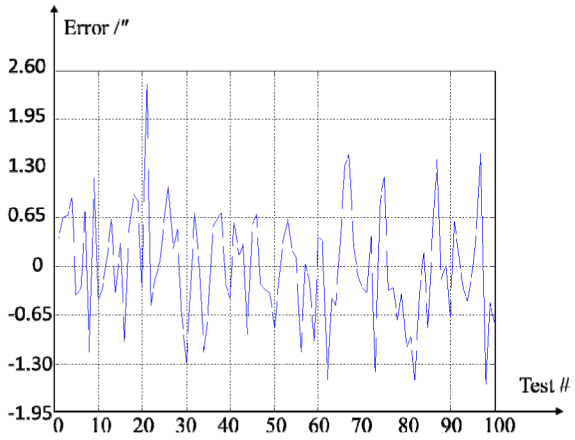

Fig. 9. Error statistics of sun sensor performance test for 100 times.

#197267 - $15.00 USD Received 16 Sep 2013; revised 16 Dec 2013; accepted 17 Dec 2013; published 23 Dec 2013

The entire performance characteristics as well as physical parameters of the digital sun sensor are summarized in Table 2.

Table 2. Performance of sun sensor

Characteristics	Performance
FOV	105° × 105°
Precision	1.1″(1σ)
Resolution	0.65″
Size	96mm × 80mm × 41.5mm
Mass	182 g
Power consumption	500 mW
Update rate	1 kHz

6. Conclusion

In this paper, a novel digital sun sensor has been proposed to meet the stringent requirements of the attitude measurement. The ERS mode of a CMOS image sensor has been discussed and employed to achieve 1 kHz data update rate. Furthermore, both "positioning apertures" and "periodic apertures" have been introduced and integrated into one mask. The combination of the mask and the multiplexing detector substantially broaden the FOV of the sun sensor with a high resolution. The experimental results demonstrate that the FOV is 105° × 105° and the precision is 1.1″ (1σ). In this case, the digital sun sensor can be applied for highly precise attitude measurement at both low frequency and high frequency. Since the digital sun sensor still has the advantages of low power consumption, small size, and light mass, it can be applied in micro- and nano-satellites as well.

Acknowledgments

This work has been carried out in the State Key Laboratory of Precision Instrument Measurement, Tsinghua University under the financial support by the China National 863 Projects (No. 2012AA121503, No. 2012AA120603) and China NSF projects (No. 61377012, No. 60807004). The authors also wish to acknowledge the contributions made by Roseanne Warren for the efforts of amending the paper.

#197267 - $15.00 USD Received 16 Sep 2013; revised 16 Dec 2013; accepted 17 Dec 2013; published 23 Dec 2013